In-situ strength effects in long fibre reinforced composites: a micro-mechanical analysis using the phase field approach of fracture

T. Guillén-Hernández[a], A. Quintana-Corominas[b], I.G. García[c], J. Reinoso[c], M. Paggi[a], A. Turón[b]

[a] *IMT School for Advanced Studies Lucca, Piazza San Francesco 19, 55100, Lucca, Italy*
[b] *AMADE, Polytechnic School, Universitat de Girona, Campus Montilivi s/n, 17071 Girona, Spain*
[c] *Elasticity and Strength of Materials Group, School of Engineering, Universidad de Sevilla, Camino de los Descubrimientos s/n, 41092, Seville, Spain*

Abstract

Transverse intralaminar cracks in layers with perpendicular orientation referred to the main loading direction have a significant affection on the apparent ultimate strength of the corresponding composite laminate. This effect stems from the fact that such transverse cracks generally promote the occurrence of other failure mechanisms leading to the specimen collapse in subsequent stages of the loading process. With the aim of conducting a careful investigation regarding the onset and progression of transverse intralaminar cracking events, in this investigation, a micro-mechanical analysis of cross-ply laminates is performed. Particularly, the cross-ply laminates belonging to the family $[0_2^\circ/90_n^\circ/0_2^\circ]$ are considered via the generation of high-fidelity micro-mechanical models, which reproduce the direct representation of internal fiber arrangements using the reference results addressed in *Saito et al. 2012, Experimental evaluation of the damage growth restraining in 90° layer of thin-ply CFRP cross ply laminates, Adv. Comp Mat, 21:1,57-66.* Differing from alternative approaches, current predictions are equipped with the combined used of two fracture-based modeling methods: (*i*) the variational phase field (PF) approach for triggering crack events into the matrix, and (*ii*) the bilinear cohesive zone model (CZM) for the simulation of fibre-matrix decohesion failures. Relying on this computational methodology, the focus of this work is to analyze the influence of the transverse ply thickness (n) on the onset and propagation of damage under tensile conditions, in conjunction with the transition from micro-cracking to meso-scale damage states. For this purpose, several models are generated into the FE package `ABAQUS` using user-defined capabilities replicating configurations of specimens included in previous experimental investigations, i.e. through the consideration of different transverse ply thickness (n=1, 2, 4). Present results show the potential of the proposed methodology to predict the transverse matrix cracking phenomena and the ability and reliability for capturing the delay of the crack with thinner plies, a phenomenon which is usually denominated as *in-situ* effect in the related literature.

Keywords: Phase-Field, In-situ effect, Micromechanics, Transverse cracking, Cross-ply laminates

1. Introduction

Thin-ply laminate technologies in long fiber reinforced composite materials (usually comprising carbon- and glass-reinforcements in polymeric-based matrix, i.e. CFRP and GFRP, respectively) has emerged as a potential alternative for the production of composite components due to their ability to preclude delamination and micro-cracking phenomena prior the corresponding collapsing points. Though thin and ultra-thin plies (with up to 0.02 mm in thickness) do offer very appealing attributes, at present, there exit some unsolved issues associated with different mechanical effects in composite materials (including standard and thin-ply thicknesses) regarding their specific fracture responses. These are the cases of the effect of different laminate disposals, ply-clustering and ply thickness, among other aspects.

Email addresses: `teresa.guillen@imtlucca.it` (T. Guillén-Hernández), `adria.quintanas@udg.edu` (A. Quintana-Corominas), `israelgarcia@us.es` (I.G. García), `jreinoso@us.es` (J. Reinoso), `marco.paggi@imtlucca.it` (M. Paggi), `albert.turon@udg.edu` (A. Turón)

As a consequence of these uncertainties, the reliable strength prediction of CFRP and GFRP structures is still subjected to the use of high safety factors, due to the fact that most of the existing failure criteria, for a given failure mechanism, present some deviations with respect to the experimental data. Advocating previous experimental studies [2], it is well established that under the action of external solicitations, initial transverse crack events (due to matrix cracking and fibre-matrix decohesion) have a minor significance on the macroscopic response of the laminate. However, upon loading progression, the increase in transverse crack density leads to the degradation of the mechanical properties at the laminate level (usually associated with transverse and shear stiffness values) arising from the potential occurrence of delamination events between the adjoining plies.

Associated with the analysis of transverse fracture response, the seminal work conducted by [56] on $[0/90]_s$ laminates showed that the reduction of the 90° layer thickness provokes an increase in the critical strain for transverse cracking initiation. Therefore, for sufficiently thin 90° layers, the actual strength response of the laminate would be that governed by the 0° supporting layers, this scenario being of crucial importance for the incorporation of thin and ultra-thin plies in composite structures. This characteristic behavior is commonly denominated as *in-situ* strength response in fiber-reinforced composites. The incorporation of such effect in macro-scale models of composite laminates [59, 57] can be accounted for using the analytical procedure proposed by Camanho et al. [11, 10], recalling the fundamental concepts on Fracture Mechanics proposed by Dvorak [23, 24, 22], through the affection of the strength values associated with: (i) in-plane transverse tensile Y_T^{is} and compression Y_C^{is} effects, and (ii) in-plane shear S_L^{is} and transverse shear S_T^{is} effects. An alternative methodology is that relying on Finite Fracture Mechanics developed by García et al. [28], whereby a semi-analytical expression for the prediction of the critical strain originating the first crack onset is derived in conjunction with a rigorous size effect law depending upon the thickness of the central 90 °layer. Apart from these valuable results, García et al. [27] performed a careful overview with regard to the main models existing in the related literature addressing the *in-situ* strength effects and compared their prediction with new experiments. These models can be categorized as: (*i*) Incremental energy models [6, 29, 33], (*ii*) Dvorak-based formulations [22, 11, 41], (*iii*) statistical-based models [40, 70] and (*iv*) coupled-criterion models [39, 28]. This analysis highlighted that most of the existing models already proposed in the related literature differ from each other upon the fundamental hypotheses for their developments. In this concern, the different hypotheses already exploited led to very diverse explanations for the so-called *in-situ* strength effects in cross-ply composite laminates. Therefore, from the authors' point of view, the physical soundness of such arguments should be revisited in a consistent manner, i.e. how cracks initiate and propagate within fibrous composites at the micro-mechanical level of analysis (being this an arduous matter to trigger via the direct experimental observations).

At present, as a consequence of the advent of new numerical capabilities, a different perspective for the analysis of *in-situ* strength effects in thin-ply composite laminates concerns the exploitation of micro-mechanical models. In line with the previous discussion, the principal aim of the use of micro-mechanics is to provide a potential explanation via the reproduction of fracture patterns in terms of initiation and propagation of crack events at lower scales that can shed light to the experimental evidences presented in [62]. Specifically, Saito and coauthors [62] identified the reduction of the corresponding energy release rate as the main cause for transverse crack suppression effect and highlighting the higher crack density for thinner plies. Interestingly, Sebay et al. [64] idealized an experimental procedure enabling the transverse cracking detection via optical means with relevant results on the matter. Within this context, from a numerical standpoint, previous works analyzed the appearance of matrix cracking and fibre-matrix decohesion at the micro-scale, which are generally identified as the initial failure mechanisms under the application of external loading conditions [67]. Thus, comprehensive investigations estimating the energy release rate (ERR) of fiber-matrix debonding cracks have been conducted by several authors [15, 74, 20], whose main focuses were on the presence of secondary loadings, fibre-spacing, residual stress fields, among other factors. Comprising high-fidelity micro-structures of fibre reinforced composites, Arteiro et al. [3] developed a finite element (FE)-based framework including pressure-dependent plasticity models and cohesive zone formulations for triggering matrix and fibre-matrix decohesion failure, respectively, showing completely different failure patterns for cross-ply laminates with standard-thickness and thin-ply 90° layers in good agreement with experimental results. Futhermore, Arteiro et al. [3] identified the *in-situ* effect in transverse compression, pinpointing the assumable reliability of simple analytical

models proposed in [11]. Following a similar approach, Herráez et al. [34] estimated via computational micro-mechanics that the transverse ply strength was independent of the 90° layer thickness. In this direction, París et al. [55] addressed the investigation of the initial phases of damage of 90° plies based on Linear Elastic Fracture Mechanics concepts and precluding the potential coalescence of interface cracks throughout the polymeric matrix, where boundary element(BE)-based models with Fracture Mechanics capabilities were generated for this purpose. These authors claimed that, at these initial phases of the cracking stage, such *in-situ* effect was not captured due to the fact that evolution of the energy release rate, $\mathcal{G}_c$, of a debonding crack was not affected by the neighboring 0° layer. In contrast, Kohler et al. [36] carried out an experimental and numerical study (using an embedded multi-scale approach), whose main results showed a good experimental-numerical agreement pinpointing the occurrence of the *in-situ* strength effect.

Despite the importance in practical applications and the great deal of research that has been devoted to this topic, there exits a clear lack of apparent consensus with regard to either the possible causes generating *in-situ* strength effects or its existence. Under these circumstances, an alternative route for investigating *in-situ* strength effects via high-fidelity micromechanical models concerns the use of the phase field (PF) approach of fracture, which has been proven as a successful predictive tool for triggering complex fracture events solids and structures [8, 46, 48]. The PF approach of fracture enables the approximation of fracture phenomena in spirit of the Griffith's vision by means of the definition of a damage-like phase field variable regularizing the sharp crack representation through the inclusion of a characteristic material length scale for such regularization. The nucleation and propagation of the fracture surface is accordingly governed by an additional PDE triggering the material stuffiness deterioration via the evolution of the corresponding crack-like phase field variable [44, 21, 47]. In the last decade, the versatility of PF-methods for the imbrication of failure mechanisms from different signature and scales of observation has been extensively examined comprising fracture events in porous materials [1], short fibre reinforced composites [17], long-fibre reinforced composites [58, 32] hyperlelastic materials [38, 61], the use of global-local modeling techniques [51], to quote a few of the current applications. Particularly, and of special interest in this work, the application of PF-based techniques to heterogeneous media has been carried out in [50] using a level-set approach, and originally by the authors in [54, 12, 13] for its coupling with cohesive-like cracks. Therefore, this variational technique can be efficiently exploited for high-fidelity micro-mechanical analysis of fibre reinforced materials with focus on the onset and propagation of transverse ply cracking in cross-ply laminates.

The central objective of the present work is twofold. The first part of the current study concerns the assessment of the practicability of the phase field (PF) method for matrix fracture in conjunction the cohesive-interface crack method for fibre-matrix decohesion for the analysis of the so-called *in-situ* strength effects. The computational methodology herewith employed comprises different novelties with respect to previous investigations on the matter regarding layered CFR and GFR composite laminates [5, 34, 36]: (*i*) the nonlocal character of the fracture method for triggering matrix failure (with reduced mes-dependence pathology in comparison local models), and with strong foundations of Fracture Mechanics, (*ii*) the corresponding coupling with cohesive fracture continuing the previous work of the authors [32] but for realistic micro-mechanical domains. It is also noting that this study has a significant deterministic character since the micro-mechanical representations of the internal fibre arrangements are extracted via the examination of the micrographies provided in [62] instead of using a statistically distributed RVE as in [3]. Additionally, the second salient objective of this investigation is to provide a further insight on the micro-mechanical response composites with special emphasis on the comprehension of the different damage phases and cracking mechanisms identified for the current loading conditions. In this direction, a significant attention is devoted to the analsysis of the transition between micro-cracking events to meso-scale damage.

The manuscript is organized as follows. Section 2 outlines the principal aspects of the current computational methodology. The construction of the numerical models is detailed in Section 3, whereas the corresponding results are presented in Section 4. Finally, the main conclusions of the present investigation and prospective research activities are addressed in Section 5.

2. Computational methodology

In this section, the main aspects of the computational strategy herein employed for the micro-mechanical analysis of composite laminates is described. Prior to summarizing the characteristics of the numerical methods for triggering fibre-matrix decohesion and matrix-cracking events, it is worth mentioning that the experimental observations of transverse cracking at micro-mechanical level clearly evidenced the two main stages: an initial phase characterized by fibre-matrix decohesion events that is followed by the kinking of such interface cracks into the matrix, provoking coalescence and branching. The conjunction of these two failure phenomena from different signature finally lead to the appearance of macro-cracks at the lamina level.

This cracking sequence, i.e. the specific sequence of damage phenomena at the micro-mechanical level for this application, motivates the use of the coupling between the PF method for bulk fracture and the CZM for fibre-matrix decohesion proposed in [54, 32], which can be denoted as PF-CZ technique. Specifically, this variational approach of fracture can be simplified through precluding the affection of the interface apparent stiffness based on the damage status of the surrounding bulk (that is accounted by the phase field variable). Consequently, standard cohesive-like elements such as the previously proposed by Turón et al. [68, 69] (see the corresponding coupling with PF-methods), and those built-in in `ABAQUS`, among many others, can be employed without any loss of generality.

2.1. Phase field approach of fracture for matrix fracture

As was previously mentioned, the nonlocal PF method of fracture is considered in the current research for triggering matrix-cracking events. This fracture model is implemented as user-defined element `UEL` into the general purpose package `ABAQUS`.

Restricting the scope of the present analysis to the infinitesimal strain setting, let to consider an arbitrary body occupying a domain $\mathcal{B} \in \mathbb{R}^{n_{dim}}$, where n_{dim} is the dimension of the analysis. The displacement field is denoted by $\mathbf{u} : \mathcal{B} \rightarrow \mathbb{R}^{n_{dim}}$, whereas the strain tensor is defined by $\boldsymbol{\varepsilon} : \mathcal{B} \rightarrow \mathbb{R}^{n_{dim} \times n_{dim}}$ and the Cauchy stress tensor is denoted as $\boldsymbol{\sigma} : \mathcal{B} \rightarrow \mathbb{R}^{n_{dim} \times n_{dim}}$. Prescribed boundary conditions are given by $\mathbf{u} = \overline{\mathbf{u}}$ on $\partial\mathcal{B}_u$ and $\overline{\mathbf{t}} = \boldsymbol{\sigma} \cdot \mathbf{n}$ on $\partial\mathcal{B}_t$, satisfying $\partial\mathcal{B}_t \cup \partial\mathcal{B}_u = \partial\mathcal{B}$ and $\partial\mathcal{B}_t \cap \partial\mathcal{B}_u = \emptyset$.

The functional that recalls the fundamental basis of the phase field method for bulk fracture can be expressed as [9]:

$$\Pi(\mathbf{u}, \mathfrak{d}) = \int_{\mathcal{B}} \psi(\boldsymbol{\varepsilon}, \mathfrak{d}) \, \mathrm{d}\Omega + \int_{\mathcal{B}} \mathcal{G}_c^b \gamma(\mathfrak{d}, \nabla_{\mathbf{x}} \mathfrak{d}) \, \mathrm{d}\Omega + \Pi_{ext}(\mathbf{u}) = \Pi_{int}(\mathbf{u}, \mathfrak{d}) + \Pi_{ext}(\mathbf{u}) = \Pi_{\varepsilon}(\mathbf{u}, \mathfrak{d}) + \Pi_{frac}(\mathfrak{d}) + \Pi_{ext}(\mathbf{u}), \tag{1}$$

where $\Pi_{int}(\mathbf{u}, \mathfrak{d})$ denotes the internal contribution to the functional due to the deformation ($\Pi_{\varepsilon}(\mathbf{u}, \mathfrak{d})$) and fracture ($\Pi_{frac}(\mathfrak{d})$) processes, and $\Pi_{ext}(\mathbf{u})$ stands for the external loading contribution; $\psi(\boldsymbol{\varepsilon}, \mathfrak{d})$ is the elastic strain energy (that is affected by the phase field variable), and $\mathcal{G}_c^b$ corresponds to the bulk fracture toughness. Figure 1 depicts an arbitrary cracked body, in which sharp crack typologies are regularized within a diffusive crack zone of width l.

In the previous variational formalism, the phase field variable $\mathfrak{d} : \mathcal{B}$ x $[0, t] \longrightarrow [0, 1]$ is introduced, which allows the distinction between fully degraded, $\mathfrak{d} = 1$, and intact state $\mathfrak{d} = 0$. The specific form of the regularized crack surface renders:

$$\Pi_{frac}(\mathfrak{d}) := \int_{\mathcal{B}} \mathcal{G}_c^b \gamma(\mathfrak{d}, \nabla_{\mathbf{x}} \mathfrak{d}) \, \mathrm{d}\Omega., \quad \text{with} \quad \gamma(\mathfrak{d}, \nabla_{\mathbf{x}} \mathfrak{d}) = \frac{1}{2l} \mathfrak{d}^2 + \frac{l}{2} \left| \nabla_{\mathbf{x}} \mathfrak{d} \right|^2. \tag{2}$$

where second-order crack surface density functional $\gamma(\mathfrak{d}, \nabla_{\mathbf{X}} \mathfrak{d})$ allows approximating surface integrals defined on sharp crack surfaces by volume integrals via the exploitation of the Γ-convergence concept [46]:

$$\int_{\Gamma_c} \mathcal{G}_c \, \mathrm{d}\partial\Omega \approx \int_{\mathcal{B}} \mathcal{G}_c \gamma(\mathfrak{d}, \nabla_{\mathbf{X}} \mathfrak{d}) \, \mathrm{d}\Omega, \tag{3}$$

The above representation of a crack surface density function has been extensively used for many authors, see [8, 49, 35]. Moreover, the parameter l is identified in the related literature as the length scale

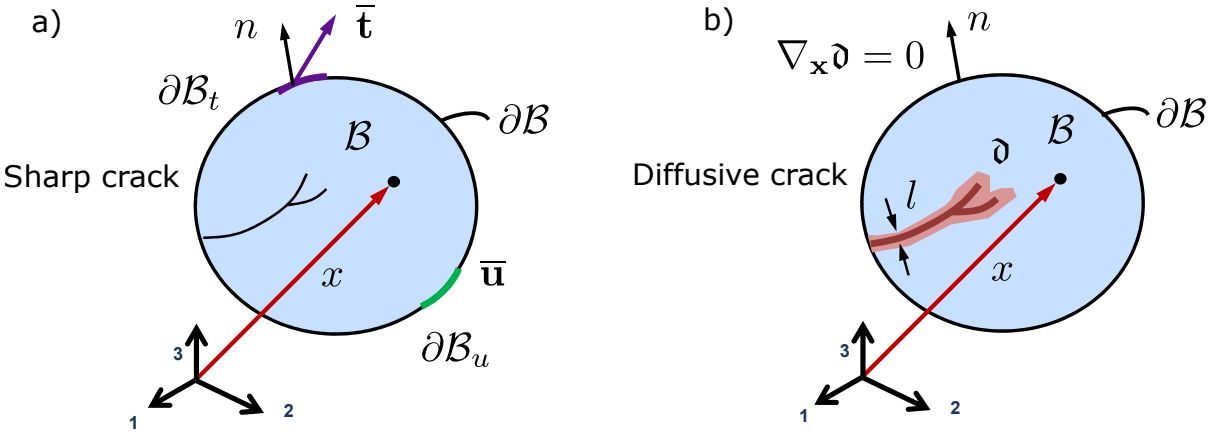

Figure 1: Phase field method for a diffusive crack modeling. a) Arbitrary cracked body with a discrete crack. b) Arbitrary cracked body with a regularized or diffusive crack.

factor, which controls the support of the transition zone of the phase field variable. This parameter can be related to the apparent strength of the material as reported in [66]. In the current formulation, l can be set for bulk fracture as follows:

$$l = \frac{27}{256}\frac{\mathcal{G}_c^b E'}{\sigma_C^2}, \tag{4}$$

being σ_C the material strength and its Young's modulus E'.

Since cracking events are different in tension and in compression, we herewith adopt the spectral decomposition of the strain tensor in its corresponding positive and negative counterparts as proposed in [46, 48]:

$$\psi(\boldsymbol{\varepsilon}, \mathfrak{d}) = \mathfrak{g}(\mathfrak{d})\psi_+^e(\boldsymbol{\varepsilon}) + \psi_-^e(\boldsymbol{\varepsilon}), \tag{5a}$$

$$\psi_+^e(\boldsymbol{\varepsilon}) = \frac{\lambda}{2}\left(\langle \mathrm{tr}[\boldsymbol{\varepsilon}]\rangle_+\right)^2 + \mu \mathrm{tr}[\boldsymbol{\varepsilon}_+^2], \tag{5b}$$

$$\psi_-^e(\boldsymbol{\varepsilon}) = \frac{\lambda}{2}\left(\langle \mathrm{tr}[\boldsymbol{\varepsilon}]\rangle_-\right)^2 + \mu \mathrm{tr}[\boldsymbol{\varepsilon}_-^2], \tag{5c}$$

where λ y μ are the Lamé constants; $\boldsymbol{\varepsilon}_+$ and $\boldsymbol{\varepsilon}_-$ are the positive and negative parts of $\boldsymbol{\varepsilon}$, respectively, indicating $\mathrm{tr}[\bullet]$ the trace operator, and $\langle\bullet\rangle_\pm$ denotes the Macaulay bracket: $\langle\bullet\rangle_\pm = (\bullet \pm |\bullet|)/2$. Following previous studies, a monotonic decreasing function is chosen for the so-called degradation function $\mathfrak{g}(\mathfrak{d})$ reads

$$\mathfrak{g}(\mathfrak{d}) = (1-\mathfrak{d})^2 + \mathcal{K}, \tag{6}$$

where $\mathcal{K}$ is a residual stiffness parameter.

With regard to the irreversible character of the crack evolution, several alternatives for enforcing such condition have been proposed in the related literature with different consequences on the reliability of the PF method, see [30] for a detailed treatment. In this work, this constraint is expressed in terms of the phase field variable using a local history field of the crack driving force [46, 73]:

$$\mathcal{H}(\mathbf{x}, t) = \max_{\tau\in[0,t]} \psi_+^e(\boldsymbol{\varepsilon})(\mathbf{x}, t), \tag{7}$$

where $\mathcal{H}(\mathbf{x}, t)$ attains the maximal value of the positive part of the elastic energy $\psi_+^e(\boldsymbol{\varepsilon})$. This new variable, $\mathcal{H}(\mathbf{x}, t)$, ensures the positive evolution of the phase field variable, i.e. $\dot{\mathfrak{d}} \geq 0$, and yields to the modification of the corresponding evolution equation of $\mathfrak{d}$. Moreover, note that this history variable is determined relying on the state variables at the pseudo-time t_i, which are constant within the time interval $[t_i, t]$.

2.2. Interface fracture model for fibre-matrix decohesion

Fracture at interfaces between fibres and matrix are modelled using built-in cohesive-crack capabilities of ABAQUS. In particular, we recall an interface crack behavior whose corresponding decohesion response complies with a bilinear traction separation law (TSL).

This TSL relates the displacement jump across the interface (identified by the normal, δ_n, and shear,δ_s contributions) with the corresponding components of the traction vector acting on it, i.e. t_n and t_s, respectively, see Figure 2 for fracture Modes I and II. This particular decohesion law follows different phases:

- An initial stage (0-1) prior damage occurrence at the interface that is characterized by a high initial stiffness K.
- Once the combination of interfacial tractions fulfills the damage initiation criterion, point 1, the interface stiffness is gradually degraded up to complete decohesion via the points 2 and 3.

As was comprehensively derived in [68], the current CZM is equipped with an internal damage variable $d \in [0, 1]$ ($d = 0$ intact interface, $d = 1$ fully debonded interface), which ensures the irreversible character of the decohesion process and tracks the progressive stiffness degradation.

Accordingly, the corresponding TSL in 2D is given by

$$t_n = (1-d)K\delta_n \;\text{ if }\; \delta_n \geq 0; \qquad t_s = (1-d)K\delta_s. \tag{8}$$

Finally, the propagation criterion for mixed-mode fracture conditions adopted is the standard quadratic criterion, see [60].

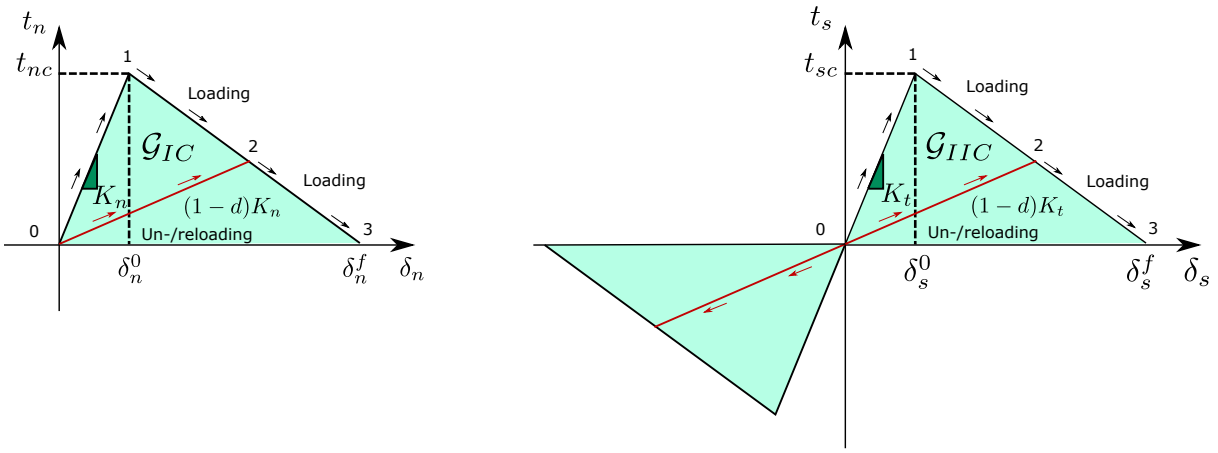

Figure 2: Bilinear traction-separation law (TSL).

3. Computational model

This section describes the generation of the micro-mechanical models under analysis. Particular details with regard to the geometry, its discretization, the loading conditions and the constitutive laws and crack modeling techniques employed for each entity are detailed and justified in the forthcoming paragraphs.

Current FE models are generated through the adoption of a high-fidelity multi-scale embedded approach similar to that employed in [45, 5, 34, 36], with the aim at replicating the experimental configurations described in [62]. Schematic description of the domains are depicted on the top of Figure 3, where the central region of interest is highlighted. As is described in detail below, the tensile loading conditions along the longitudinal directions of the specimens at the experiments are transferred to the central area via prescribed displacement conditions (denoted by δ_x in Figure 3). Excluding grip tabs, the specimens correspond to standard cross-ply laminates, which are composed by three layers: two outer layers (0°

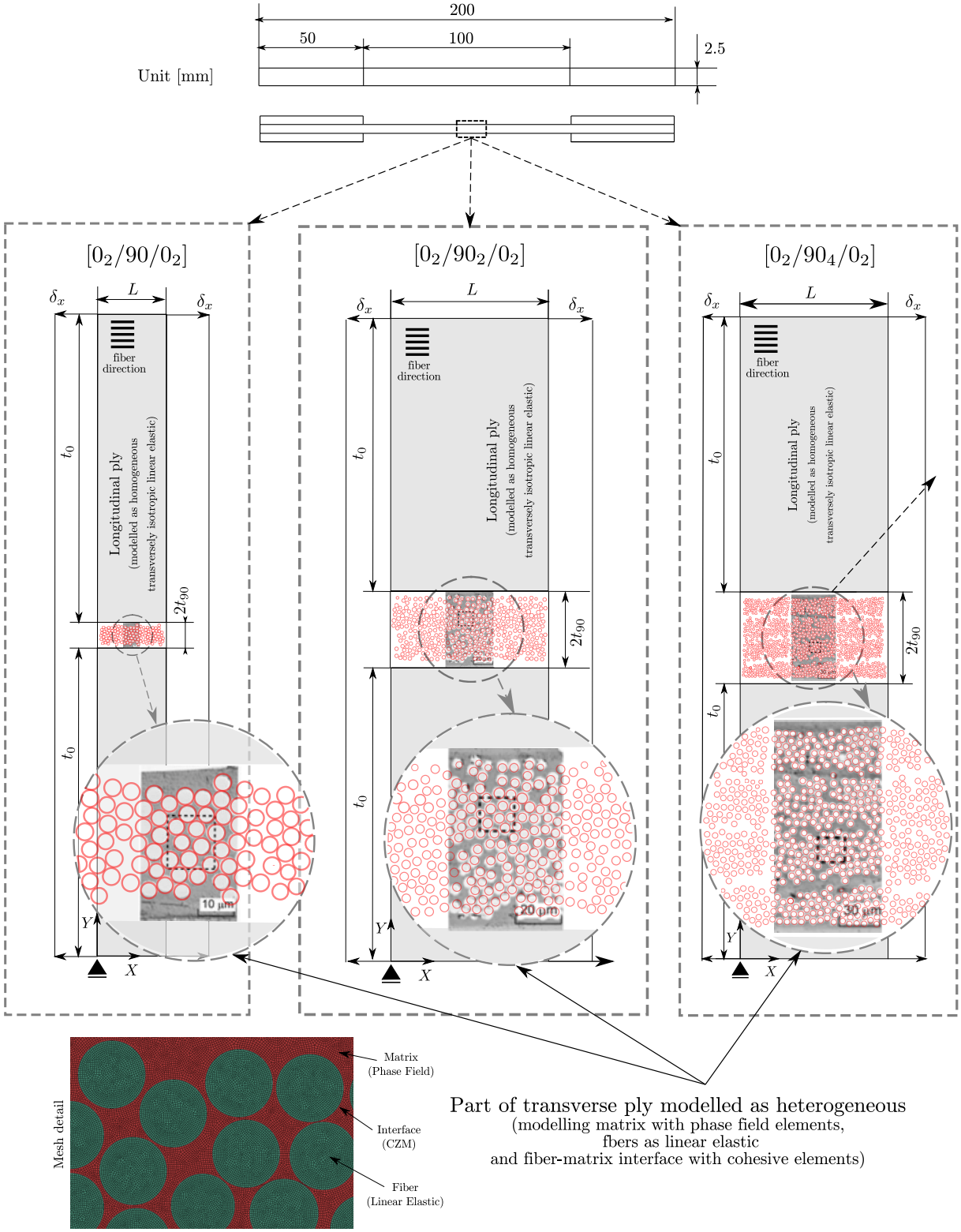

Figure 3: Details of the computational models generated to simulate the [62] experiments

layers) with fibers orientated along the loading direction, and a central layer with fibers perpendicular to the loading direction (90° layer). Note that the present simulations comprise a sufficiently long section

for each specimen using a plane strain formulation, see Figure 3, and whose respective dimensions are reported in Table 1. As can be observed in this graph, three different models are generated according to the three types of specimens tested in [62]. The difference between these three models relies on the thickness of the central 90° layer, ranging from 0.04 mm to 0.16 mm. In contrast, the thickness of each individual 0° layer is equal to 0.24 mm. Thus, the stacking sequences of the current models correspond to: $[0^\circ_2/90^\circ_n/0^\circ_2]$ being $n = 1$, 2 and 4. Note that 0° and 90° layers are composed by plies with different thickness. Therefore, the notation [0/90/0] can be confusing but it will be used here to keep the notation used in the experiments [62].

Material	E [GPa]	ν	$\mathcal{G}_C$ [N/mm]	l [mm]
Fiber	13	0.2	-	-
Matrix	2.79	0.33	0.02	0.00105

Material	E_{11} [GPa]	E_{22} [GPa]	E_{33} [GPa]	ν_{12}	ν_{13}	ν_{23}
Homogeneous 0° ply	113.5	8.31	8.31	0.3	0.3	0.45

Interface Property	σ_C [MPa]	$\mathcal{G}_C$ [N/mm]
Fracture Mode I	75	0.002
Fracture Mode II	100	0.04

	$[0_2/90/0_2]$	$[0_2/90_2/0_2]$	$[0_2/90_4/0_2]$
Laminate length [mm] (L)	0.4	0.8	1.6
90° layer thickness [mm] ($2t_{90}$)	0.04	0.08	0.16
0° layer thickness [mm] (t_0)	0.48	0.48	0.48

Table 1: Material properties [62, 4, 42] and geometrical parameters of the $[0^\circ_2/90^\circ_n/0^\circ_2]$ ($n = 1$, 2 and 4) laminates.

Focusing on the central parts of Figure 3, for each configuration, the geometry is composed by three entities (regions), representing the three layers. The outer 0° layers are modelled as homogeneous solids, whereas for the 90° layers, the actual micro-structure is specifically taken into account. This is performed by modeling such domains as heterogeneous regions with two different phases (i.e. fibres and matrix) and the corresponding interfaces. These micro-structures are identified by means of an in-house Python script that allows the rapid transfer of the geometrical information for the subsequent operations in the modelling process to be performed. Nevertheless, note that due to the fact that a reduced region of the microscopic fibre distribution is available in [62] for each configuration, the corresponding representative region of the micro-structure is defined and reproduced throughout the 90° plies in order to preclude undesirable edge effects upon loading.

Regarding mesh details, at the micro-mechanical level, very finely discretized 90° plies are generated (Figure 3). These dense meshes are constructed in order to fulfill with the requirements of the different constitutive laws applied to each part of the geometry. In particular, the mesh is fine enough in the *Observed area*, in order to adequately model the process of crack events which occurs at this zone.

With reference to the simulation capabilities, different modeling techniques are defined within the models, which are selected in terms of several arguments: (i) the nature of the region itself, (ii) the typical failure behavior, and (iii) the level of interest of the region:

- The 0° layers are modelled as homogeneous orthotropic linear elastic solids with the material properties detailed in Table 1. No damage is expected to occur in these layers during the firsts stages of the failure mechanism herewith studied. Thus, a linear elastic constitutive law is considered to adequately represent the mechanical performance of this region of the models.

- Interface behaviors between 0° and 90° layers are simulated as a perfect interface. It is well known that the failure mechanism studied here leads to subsequent delaminations between such layers [7]. However, this mechanism is out of the scope of the present study.

- Fibers in the 90° layer are modelled to follow an homogeneous isotropic linear elastic response. Fibers actually obey a transversely isotropic response. However, within the current plane strain formulation, their mechanical performances are assumed to comply with the corresponding equiva-

lent plane strain properties, see Table 1. Similarly to the 0° layers, no damage is expected to occur inside the fibers during the first phases of the failure mechanism studied in the present study[1].

- Matrix within the 90° layers is modelled as homogeneous and linear elastic isotropic entities. During the failure processes, damage and cracks are expected to progress within the matrix, so it is required to reproduce such cracking phenomena with a proper level of reliability. In this direction, it is worth mentioning that modelling of crack events at the micro-scale level is very challenging and complex because such cracks progress from very short cracks, whose failure is governed by a stress criterion, to large cracks, whose failure is mainly governed by the classical Griffith energy criterion (LEFM). Thus, in our vision, modelling matrix crack events either using LEFM (which it is not able to accurately predict the behavior of small cracks at this scale) or a stress-based criterion, via e.g. a combination of damage-yielding model, (that it is not able to predict well the behavior of large cracks) might present significant limitations. In order to overcome these issues, the adoption of robust numerical frameworks that enable predicting both behaviors is a matter of enormous importance. In this concern, cohesive zones models (CZMs), finite fracture mechanics (FFM), or phase field (PF) can be understood as suitable modeling tools for crack events which fulfill with the previous requirements. In particular, these three approaches have been assessed for recovering both extreme scenarios (stress- and energy-dominated crack phenomena) and the transition between them with excellent results, see [14, 66]. Thus, for the matrix cracking, since the crack paths are a priori unknown, the phase field (PF) strategy described in Section 2.1 is herewith exploited due to its extraordinary capabilities in terms of reproducing very complex crack paths without the use of arduous re-meshing and crack tracking methodologies in the corresponding FE implementation.

- In addition to matrix-dominated cracks, based on experimental observations, failure mechanisms in the current specimens presented significant fibre-matrix debonding events [62]. In order to model such phenomena, fiber-matrix interfaces within the 90° layers are modelled using CZMs as described in Section 2.1, obeying a bilinear TSL. Note that, similarly to the matrix, in this case, the average fibre-matrix crack size is small enough to be comparable to the fracture process zone. Thus, a predictive approach based exclusively on a LEFM analysis would present some limitations for the accurate estimation of the crack growth along the fiber-matrix interface. Interfacial cohesive properties are detailed in Table 1 and the interface initial stiffness K is set equal to 1×10^8 [MPa/mm] for fracture Modes I and II [4].

Regarding the prescribed bounday conditions, in line with the previous description, the external solicitation corresponds to prescribed horizontal displacements δ_x at the left and right extremes of the models. A fixed loading increment is prescribed, which is directly proportional to the individual model length L, in order to keep constant the corresponding strain increment for each model. In addition, a point is fixed at the left bottom corner in order to avoid rigid motions.

Finally, due to the fabrication procedure of the actual specimens, it is expected to find a certain level of residual thermal stresses within the domain at the layer scale. Thus, the strain levels advocated in the present results are computed in such a way that the consideration of the residual thermal stress are already incorporated. These thermal effects are calculated according to the procedure described in [26].

4. Results and discussion

This section presents the results obtained from the computational models corresponding to the micro-mechanical response of the cross-ply laminates described above. Furthermore, the present section addresses a comprehensive discussion in terms of the reliability and capabilities of the current numerical methodology.

The objective is to investigate the process of initiation of a crack from the very first form of damage to a crack spanning the whole 90° layer, which can be already considered a meso-mechanical crack. The

[1] Actually, some micrographies show rarely transverse breaks of fibers, but the relevance of this phenomenon is not common enough to be of remarkable significance in the failure process. In fact, no fiber breakage was reported in [62].

influence of the 90° layer thickness on this process is also analysed through the comparison of the present estimations for the three specimens with different thickness values and with respect to the available experimental data [62]. Furthermore, it is of remarkable interest the way through which cracking events evolve at the micro-scale of the current models, since they provide a very valuable information in terms of the nature of damage progression. The careful analysis of the simulation data herein conducted can lead to a plausible understanding of the causes of the *in-situ* strength effect.

The forthcoming discussion is articulated in three individual stages based on the sequence of damage events identified throughout the simulations. First, the process of cracking initiation is analysed for each specimen, focusing on the different phases at the micro-mechanical level. Second, the computational results are correlated with the experiments reported by Saito et al. [62]. Finally, the results are discussed in a global context, specifically, paying special attention to the comparison with respect to different models already proposed in the related literature.

4.1. Process of crack initiation at the layer scale from a micromechanical analysis: from micro-mechanical cracking to meso-scopic damage

The detailed analysis of the progress of damage and cracks within the current micro-mechanical models clearly reveals the different phases of failure processes (Figures 4-7). Specifically, failure maps corresponding to the interface damage variable and phase field-crack at the matrix are shown in Figures 4, 6 and 7, pinpointing the different cracking sequences (identified by numbers) which are represented by the damage variables for fibre-matrix delamination and matrix failure. As expected and in line with the experimental observations [62], cracks principally evolve along the direction transverse to the external loading. The comprehensive description and discussion with regard to the different phases of the crack events for the three specimens under analysis is outlined as follows:

- First, according to the computational results, the first damage event corresponds to the onset of a debond at the fiber-matrix interface (labelled as phase 1 of the crack evolution in Figures 4, 6 and 7). The position of this debond occurs at the zone of the interface where the normal stresses achieve the corresponding highest levels, which is generally identified at narrow portions of the matrix between fibres [4, 3]. Advocating previous studies regarding the stress solution for a circular inclusion in a infinite domain under remote tensile stress [31], the critical point for such decohesion corresponds to one of the poles leading to a non-symmetric post-failure configuration. This event is accurately captured by the current simulations since this initial debond is predicted to occur at one of the two critical locations (phase 1) [25]. Moreover, it has been extensively reported that the very first initial debonding process is an unstable phenomenon but it becomes stable in subsequent stages [32, 43, 25]. This development (unstable-stable) is a direct consequence of several factors comprising the transition from fracture Mode I to II along the interface, the mismatch between the mechanical properties of the fibre and the matrix, among others.

- The second fracture stage identified in computational results is the appearance of several debonds at different fiber-matrix interfaces (phases 2 and 3 in Figures 4, 6 and 7). These interface cracks can take place relatively far from the first debond, but depending upon on the particular fibre positions. The reason for this event is attributed to the fact that the stress state around an intact fiber-matrix interface is very similar for most of the fibers (for the prescribed tensile loading), but with slight modifications due to geometrical aspects associated with the micro-structural arrangement, e.g. relative position of the neighbouring fibers [65, 63]. Thus, several fibers with similar situations in terms of stresses, can be found in a micro-structural system. Correspondingly, for a certain strain level, it is expected to observe several isolated debonds. It is also noting that such debonds are prone to occur at the fibers with a preferential neighbouring situation, which promote the occurrence of such failure. Moreover, in all the cases here analyzed, the fibre-matrix damage progress at different locations up to their corresponding critical conditions prior to kinking towards the matrix [32], this effect being in good agreement with experimental observations.

- The third phase observed in the present simulations can be already considered as an initial stage of damage which can have a noticeable relevance at the meso-scale (phases 4 and 5 in Figures 4, 6 and 7). The presence of fiber-matrix debonds notably alter the stress state at such locations,

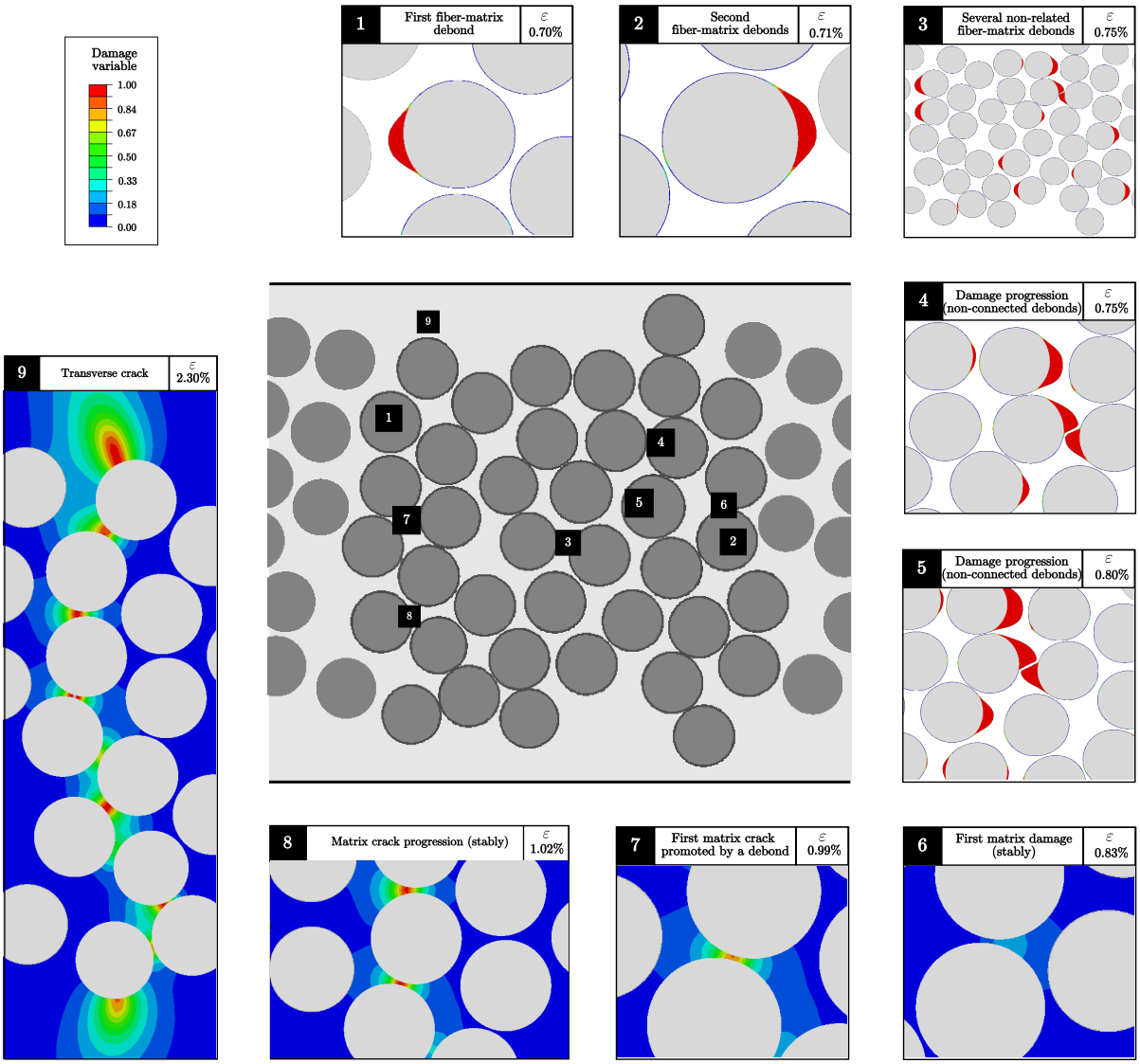

Figure 4: Sequence of damage events observed in the computational results for $[0_2/90_1/0_2]$ laminate.

leading to two possible alternative scenarios upon fracture progression: (i) the further promotion of the fibre-matrix debonding in neighbouring fibres, or (ii) the protection of nearby fibre-matrix interfaces. This idea is illustrated in Figure 5, whose main conclusions are summarized:

- In situations where a first exemplary debond is initiated at a particular location (1), in posterior loading stages, a second debond can take place at a different fiber (2), which is relatively far from the first one (complying with the second scenario aforementioned). The reason for which these first two debonds take place at these particular locations is directly attributed to the particular arrangement of fibers. Notwithstanding, in the case of numerical studies based on statistical distributions of interface fracture and strength properties, the particular location of the first debond would be also affected by this scatter.
- Continuing the analysis and evidencing the concomitant occurrence between the promoting and protective interface failure mechanisms, which depend on the status of surrounding fibres, it is observable that: whereas the fiber-matrix interface failure at fiber (1) evolves in a larger damaged zone with other neighbouring debonds aligned with the main loading direction, the debond at fiber (2) does not promote any further interface cracks at its surrounding area.

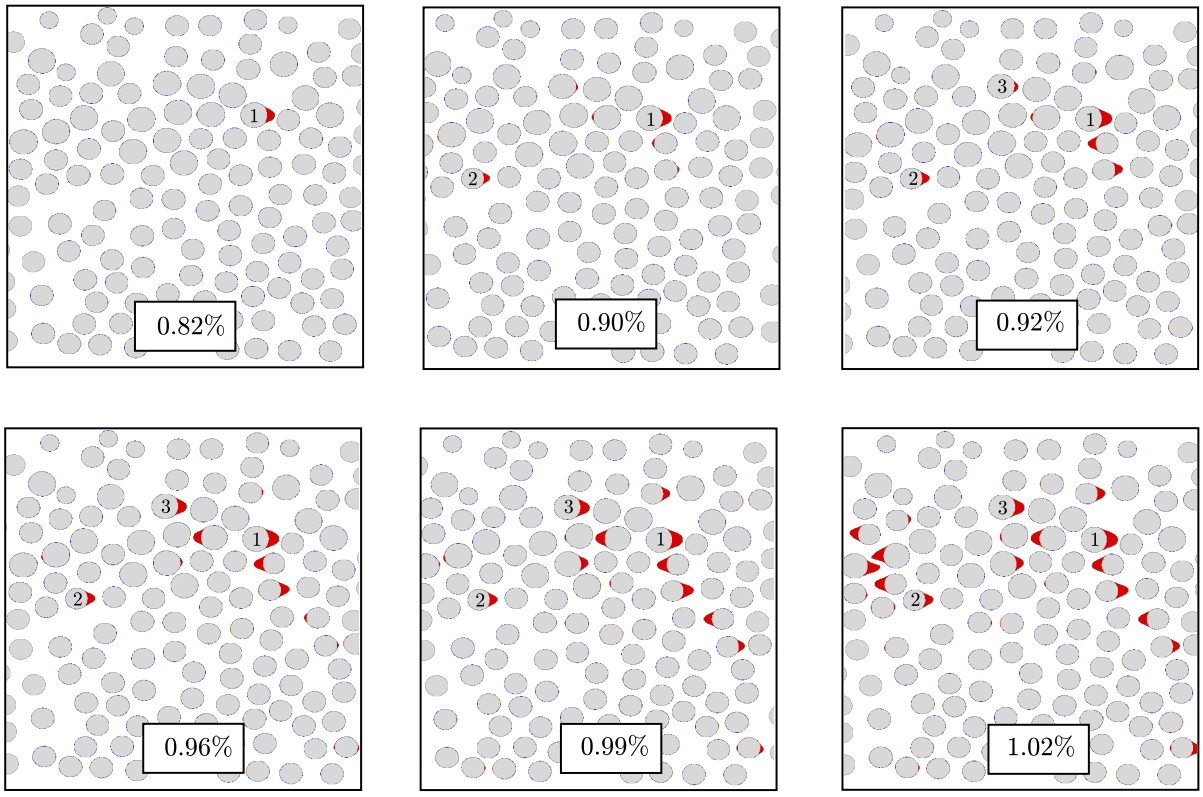

Figure 5: Detail of evolution of debonds at the first stages of damage initiation for $[0_2/90_2/0_2]$ laminate. Values showed in labels correspond to the strain level.

(Figure 5). In fact, subsequent debonds, as that identified by (3) in this graph, contribute to the progression of additional interface failure phenomena. Note that the connection between such debonding failure at the micro-scale may produce a meso-scale crack event.

Once the damaged regions (formed by aligned debonds) have been clearly developed, the progress of such phenomena is diverse. At this phase, several fibre-matrix debondings can further propagate in a stable manner up to the attainment of the next energetic barriers, which can correspond to the relative positions of the fibres, the presence of resin-rich regions, among others. Note that these energetic barriers are statistically distributed within the domain based on its own internal arrangement. The delay in posterior damage propagation leads to accumulation of energy within the system, so that such energetic barriers can be overcome leading to unstable (sudden) damage evolution.

- The next stage here identified comprises the fact that fibre-matrix interface failures generally span the whole thickness of the 90° layer. This happens prior the occurrence of any crack kinking phenomenon towards the matrix in the whole thickness of the 90° layer as is shown in Figures 4, 6 and 7, and subsequently in Section 4.2. This behavior strongly depends on the corresponding matrix and fibre-matrix interface fracture properties.

- Upon loading progression, significant damage matrix events are predicted at the micro-scale, which, as expected, take place in the neighbourhood of several fibre-matrix debond tips (see phase 6 in Figures 4, 6 and 7). This is the previous step to the appearance of a matrix crack promoted by the fiber-matrix debonds. Since the size of the process zone in this problem is of the order of the fiber radius, it is expected to have a significantly large damaged zone before the corresponding kinking phenomenon.

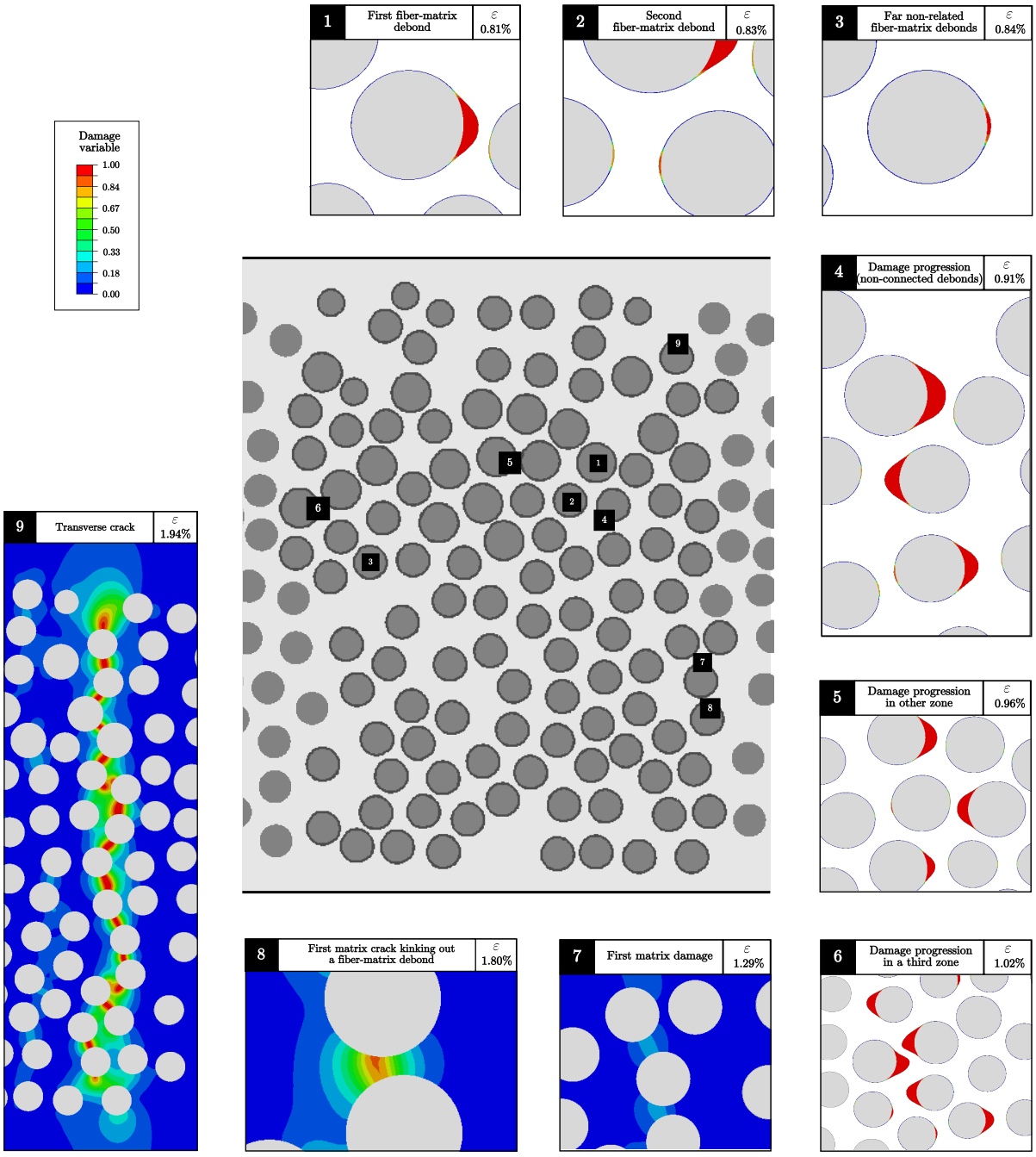

Figure 6: Sequence of damage events observed in the computational results for $[0_2/90_2/0_2]$ laminate.

- The posterior stage concerns the nucleation of a matrix crack in the damaged zone near a debond tip (see phases 7 and 8 in Figures 4, 6 and 7). This matrix crack connects two debonds of neighbouring fibers. The preferential path is mainly perpendicular to the loading direction, in consonance with the experimental evidences [62] and alternative numerical studies [3, 34]. However, the specific direction is mostly governed by the connection between the debonds already existing at the fibers.

- Once the first matrix crack appears connecting two debonds, this crack progresses up to spanning almost the whole thickness of the 90° layer (stage 9 in Figures 4, 6 and 7). This crack can be already considered a damage event at the meso-scale. Thus, this phase can be considered as the final

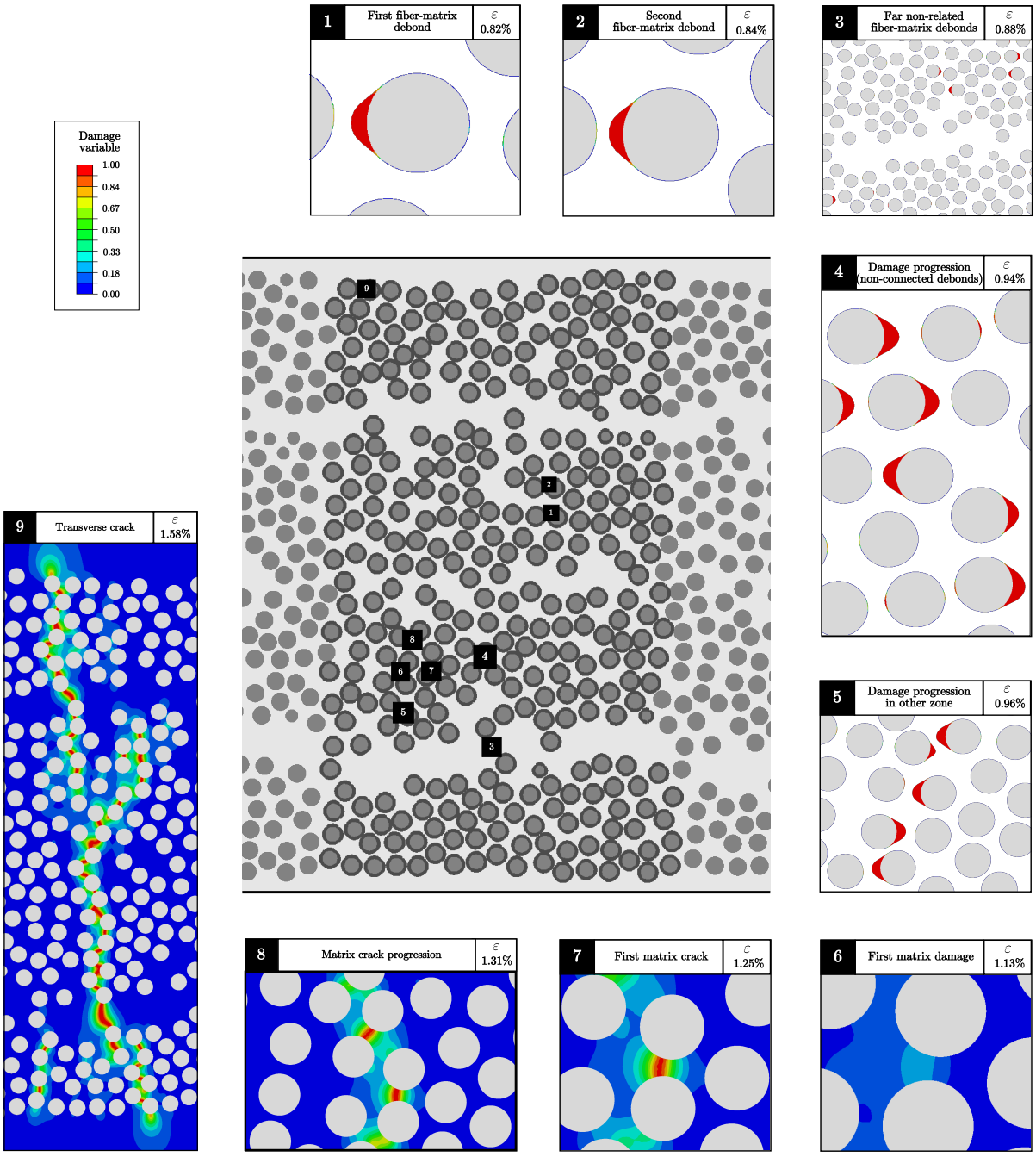

Figure 7: Sequence of damage events observed in the computational results for $[0_2/90_4/0_2]$ laminate.

transition between micro-scale cracking and meso-scale damage. The stability of this progression is mainly ruled by the presence of energetic barriers which interrupt further progressions. Current computational results predict that this process is generally unstable with some differences depending on the 90° layer thickness. It is also interesting to observe the final geometry of the fully transverse crack. Thus, in the case of the 90° layer would have been studied as an equivalent homogeneous solid, the preferential crack geometry would correspond to a straight crack perpendicular to the loading direction. However, this is not exactly what it is observed in the computational results presented here. At the micro-mechanical level, the actual heterogeneity of the specimen, in particular when some damage events have occurred, e.g. the distribution of debonds, promotes alternative crack

paths with more chaotic topology. This is particularly significant for the thickest laminate here analyzed, see Figure 7.

4.2. Comparison with experimental results

This section outlines the comparison between the experimental results in [62] and the predictions obtained from the current computational models. The main target is to assess the influence of the 90° layer thickness on the onset and propagation of through-thickness cracking events in line with [34, 4, 3]. The current correlation relies on performing a comparison between the three states reported by Saito et al. [62] for each model (corresponding to three strain levels) with respect to similar damage extents in the current computations. Correspondingly, it is possible to compare the strain levels for which the computational models predict "similar" damage levels to those reported in the experimental study. Note that this comparison is focused on the analysis of the micrography given in [62]. Moreover, it is worth mentioning that the 2D simulations here presented cannot take into account "tunneling effects", and therefore deviations with respect to the experimental data are expected in terms of characteristic strain values and cracking topology. These deviations are also affected by the deterministic character of the study.

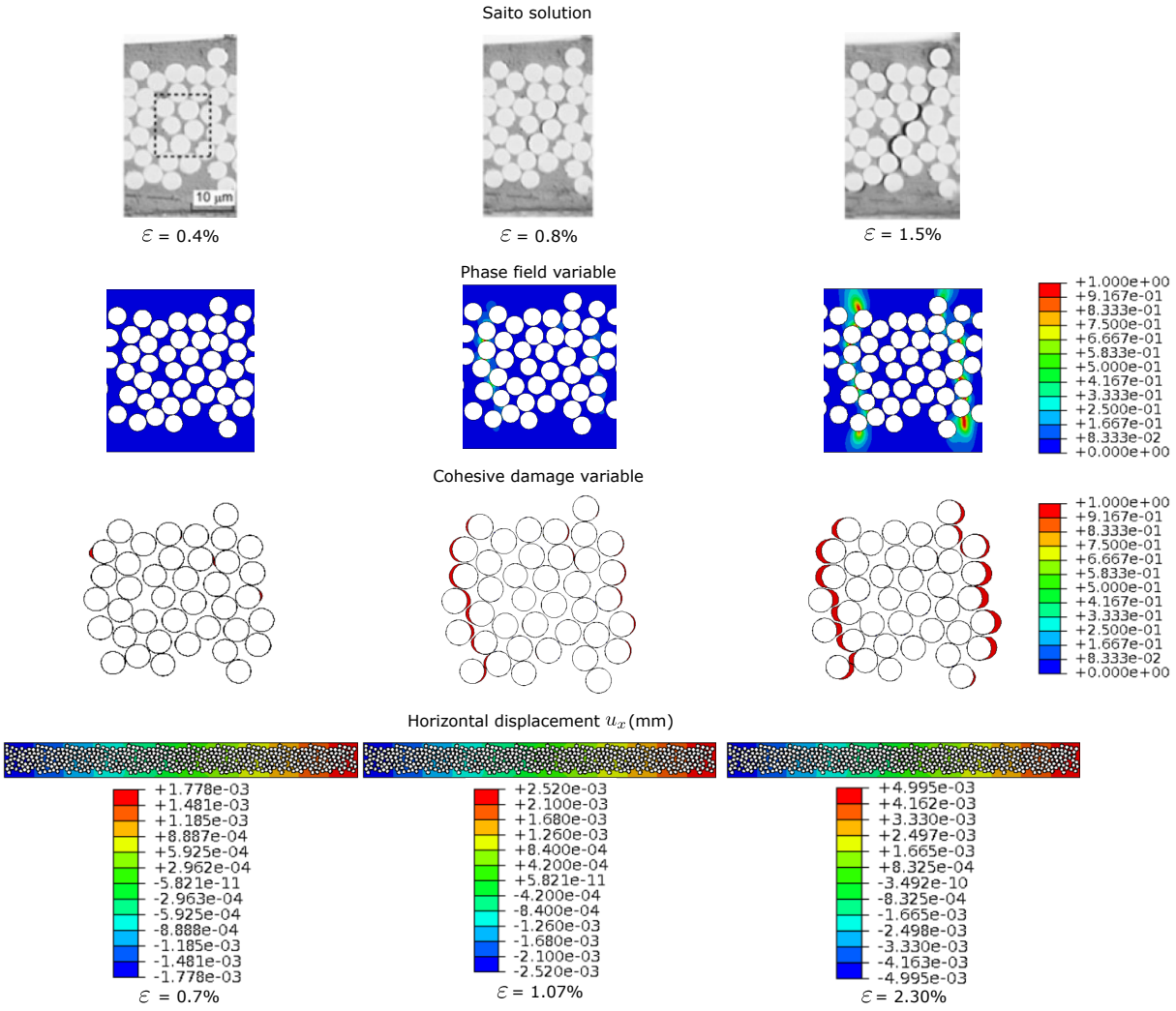

Figure 8: Saito [62] $[0^\circ_2/90^\circ/0^\circ_2]$ laminate results: Saito results, strains (ε), damage patterns, debondings and contour plot of the horizontal displacement field.

Figure 8 presents the comparison for the thinnest laminate with 0.04 mm in thickness of the 90° layer. As discussed in the previous section, damage started by the fibre-matrix interface debondings, which

subsequently progressed in neighbor fibres and finally kinked towards the matrix forming a through-the-thickness crack. This sequence of cracking events is correctly reproduced by the present simulations. Thus, the first column of this graph corresponds to the appearance of the first debonding event at the fibre-matrix interface, which was identified in the experiment at a strain level of $\varepsilon = 0.4\%$, whereas the current computational model predicts the first debond at $\varepsilon = 0.7\%$. As the applied strain increased, subsequent damage states evolve. Thus, the second column is reffered to the first cracking state formed by several aligned debonds. According to the experiments, this occurred for $\varepsilon = 0.8\%$ whereas a strain level equal to $\varepsilon = 1.07\%$ is identified for predictions of the computational model. Finally, the third column identifies a crack spanning almost the whole thickness of the 90° layer, this taking place for $\varepsilon = 1.5\%$ in the experiments whereas the similar status is achieved at $\varepsilon = 2.30\%$ according to the computational model.

Note that the position of the damage and cracking events notably diverges from the experimental observations to the computational estimations. As was amply discussed in previous studies, this result is expected because this is the classical problem of multi-site nucleation for damage, where many very similar points with critical conditions there exist, such locations being of potential damage initiation. In this case, these points corresponds to the fiber-matrix interfaces with a very similar situation between them at the beginning of the failure mechanism. Therefore, the point at which the damage is finally nucleated at first is determined by very slight differences in geometry, elastic, strength and fracture properties. The geometry is the only source of such diversity in the current computational model and not completely, due to the fact that small differences in the distributions of fibers at alternative placements of the laminates can affect the occurrence of this phenomenon.

As for the strain level, the comparison shows a certain level of divergence between the experiments and the computational model. The difference can be associated to the influence of the 3D effects, i.e crack tunneling aspects. In particular, these effects can be very relevant for the first debonds occurring at the free edge locations. The problem in this initial stage is therefore highly 3D due to a high stress concentration due to the different properties of fiber and matrix and the presence of a free edge. For the second and third column, the agreement between the experimental and the numerical data is similar to the first stage, likely promoted by the same effect.

Figure 9 depicts the comparison for the intermediate in thickness laminate, i.e. 0.8 mm in thickness of the 90° layer. With respect to the damage pattern, the first column shows the very first debond, which occurred at a strain level of $\varepsilon = 0.4\%$, whereas the computational model predicts this event at $\varepsilon = 0.81\%$. In the second column, the first damage formed by several aligned debonds can be observed. According to the experiments, this took place for $\varepsilon = 1.2\%$, whereas the computations predict this event at $\varepsilon = 1.83\%$. Finally, the third column correspond to a crack spanning almost the whole thickness of the 90° layer, this happening for $\varepsilon = 1.3\%$ in the experiments and $\varepsilon = 1.88\%$ according to the computational model. Note that the criterion about the prediction of the situation for damage and crack initiation also holds for this model. In this configuration, experimental and computational model results present notable deviations. These discrepancies are mainly attributed to the specific damage identification criterion herewith adopted.

Figure 10 presents the comparison for the thickest laminate, complying with 0.16 mm in thickness of the 90° layer. In line with the previous results, the first column of this graph corresponds to the appearance of the first debond, which occurred at a strain level of $\varepsilon = 0.7\%$ in the experimental study [62], whereas the computational model predicts the first debond at $\varepsilon = 0.82\%$. The second column stands for a state with the presence of transverse crack identified by the presence of multiple fibre-matrix debondings. According to the experiments, this occurred for an applied strain equal to $\varepsilon = 1.0\%$, whilst this situation is achieved in the current computations for $\varepsilon = 1.32\%$. The third column identifies a crack spanning almost the whole thickness of the 90° layer, this happening for $\varepsilon = 1.4\%$ in the experiments and $\varepsilon = 1.58\%$ according to the computational model. For this model the agreement between the computational model and the experiments is better than the previous ones. This could be connected with the idea of that failure for thin laminates is more governed by 3D phenomena (not taken into account here) than for thick laminates, as claimed by some works [23, 24].

Once the current results have been described and contrasted with respect to available experimental data from a quantitative standpoint, it is interesting to perform a qualitative discussion of the predictions. In this context, it is noting that the *in-situ* observations reported in [62] identified that, for thicker 90° layers, the formation of a transverse crack experiences a rapid propagation through-the-thickness. This

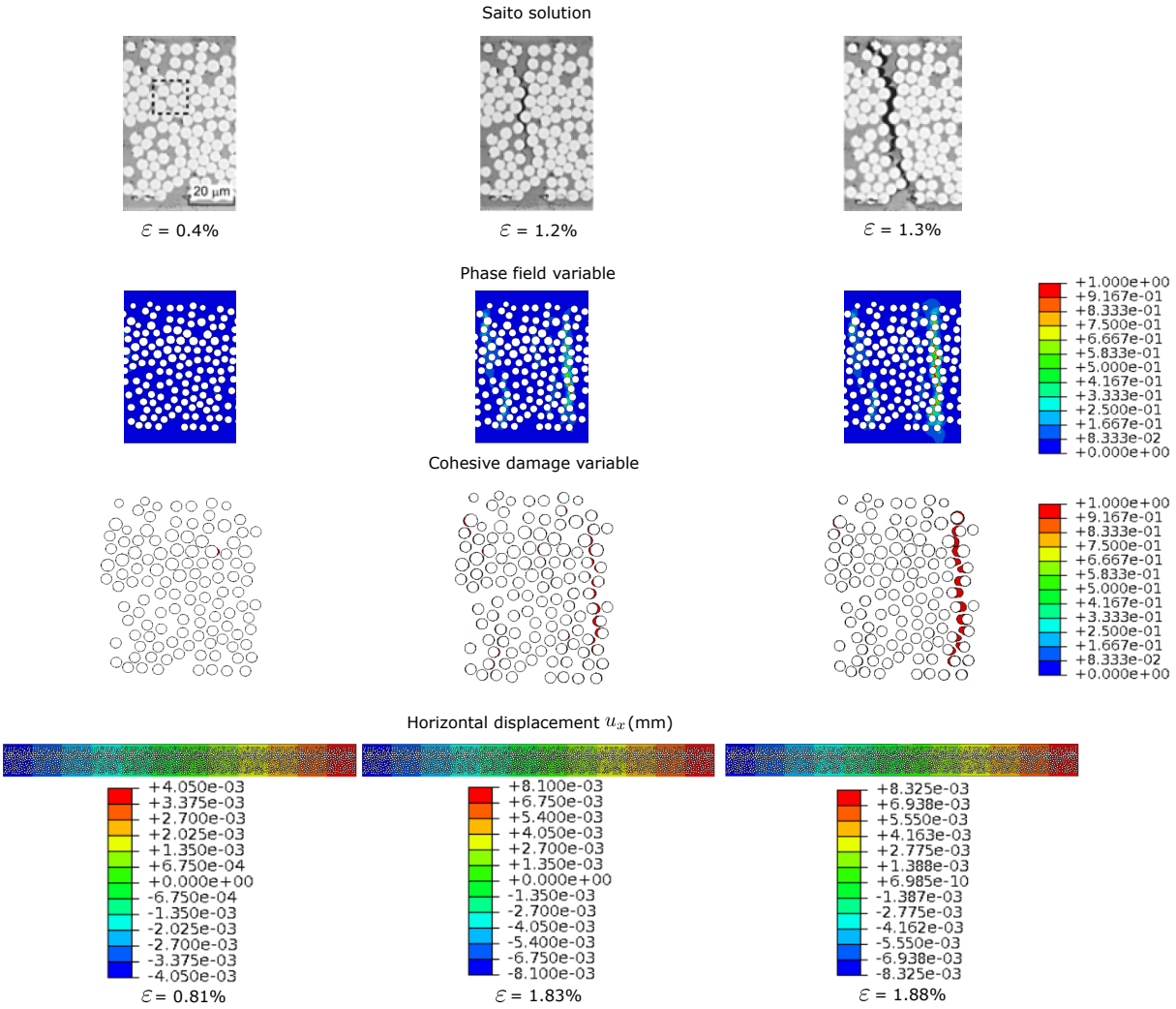

Figure 9: Saito [62] $[0_2^\circ/90^\circ/0_2^\circ]$ laminate results: Saito results, strains (ε), damage patterns, debondings and contour plot of the horizontal displacement field.

contrasts with the case of the thinnest specimen, whose simulations exhibits a more stable through-the-thickness crack propagation with increasing values of the applied strain, leading to higher values of the final failure strain. This trend is well captured in the present predictions, with the capacity of simulated damage events of different signatures and extent with physically-sound fracture models.

4.3. Size effect of the 90° layer. Comparison with the main theoretical models

This section analyses the role of the 90° layer thickness on the different steps of the failure mechanism, from the first fiber-matrix debonding event to the full transverse crack. Therefore, the current discussion allows the assessment of the *in-situ* strength behavior in conjunction with tracking the transition between micro-cracking to meso-scale damage scenarios.

Figure 11 reports the strain level at which the main characteristic phases of the failure mechanisms are identified in the computational results as a function of the 90° layer thickness.

For the first step, which corresponds to the initial fiber-matrix debonding failure, it can be observed that the strain level is almost independent of the 90° layer thickness. The reason for this is clear, this event is mostly sensitive to the elastic properties of fiber and matrix, fracture properties of the interface and fibers radius, see e.g. [42]. Since these parameters are very similar to each other for the three models herein presented, it is expected to obtain a similar strain level for this first event. Note however that, in a

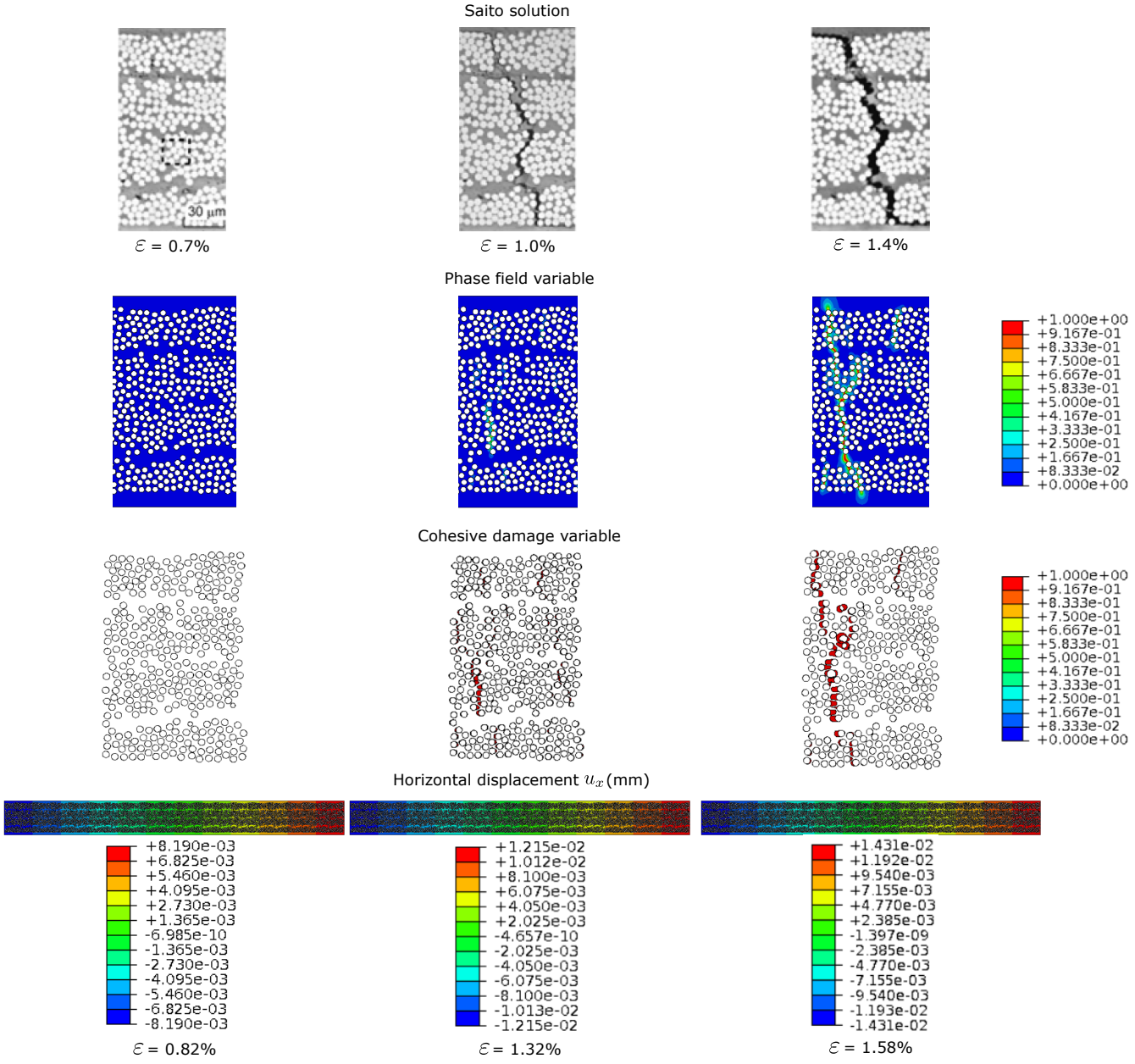

Figure 10: $[0^\circ_2/90^\circ_4/0^\circ_2]$ laminate results: damage pattern, contour plot of the horizontal displacement field and strain (ε).

lower level of influence, the situation of the neighbouring fibers can also play minor influence. Thus, the presence of more preferential situations in some models or slight micromechanisms of stress concentrations as fiber clustering is the main source of the slight differences between the current computations.

For the second event, which stands for the first debond kinking out towards the matrix presents an interesting size effect: the lowest value of the strain is found for the thinnest laminates, whilst the highest strain for the intermediate in thickness laminates. Note that current simulations predict nonuniform evolution since this phenomenon has a notable influence of the specific internal arrangement of the material, i.e. fibre locations, matrix-rich regions, among other aspects.

Interestingly, for the transverse crack a monotonic size effect can be identified, from the thinnest laminate to the thickest one, the size effect complies with the classical size effect reported by Parvizi [56] and subsequent experiments [53, 52, 27]. This trend exhibits a decreasing evolution of the critical strain leading to a first through-the-thickness transverse crack as the 90° layer thickness increases. The reason

for this size effect can be understood by comparing the evolution of the three stages plotted in Figure 11. Whereas first and second stages are very dependent on scattering on fibers arrangements, the third stage is significantly affected by the energy available to be released in a potential crack propagation. Thus, the key point is the nature of the damage evolution from the very first crack kinking out the fiber-matrix interface towards the matrix up to the full transverse crack. Once the first kink out occurs, the nature of this damage evolution is going to depend on the elastic energy available to propagate this crack up to span the whole thickness. For thinnest laminates, even if the first kink occurs prematurely, the elastic energy available to be released is low and the progression requires a significant increase of strain. In contrast, for the other laminates the increase in strain from second to third stage is significantly lower, showing a behavior much more unstable. In fact, for the thinnest laminate, it is not expected that this stable evolution can be detected by acoustic emission, which is the classical method used to detect transverse cracks in experiments. This crack would be likely detected in a subsequent stage of propagation as tunneling crack, which would be unstable in the last stage.

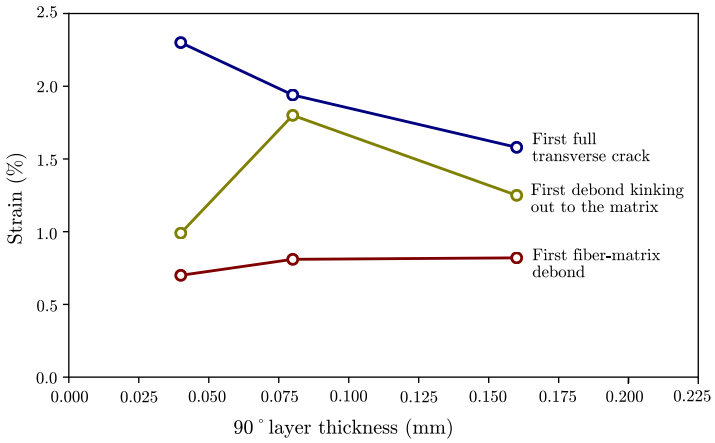

Figure 11: Effect of the 90° layer thickness on the strain for which the different steps of the process of crack initiation are observed in the computational model

Beside the previous discussion, it is interesting to analyze the results summarized in Figure 11 advocating previous theoretical models in order to explain the size effect observed in classical experiments, see the review outlined in [27].

One of the most accepted model in the related literature is the so-called Dvorak's formulation [24], which is based on assuming that a damage zone grows stably up to a certain critical length where it commences to progress unstably. Under such conditions, the critical length is assumed to be a material property. Very succinctly, the relation between this critical length and the 90° layer thickness promotes the size effect and differences on the crack growth direction (which can evolve either as a tunneling crack or a transverse-thorugh the thickness crack), see [24] for a detailed justification. The weak point of this model relies on the hypothesis of the existence of a "material critical length" governing the transition from stable to unstable crack growth. It is interesting to observe that the transition has been identified here, see discussion in Section 4.1. However, the relation between the transition and a critical length could be certainly concluded. In addition, it is worth noting that the nature of crack growth between the first kink and the first transverse thorugh-the-thickness crack in Figure 11. The evolution is much slower for the thinnest laminate than for the other two laminates, experiencing a clear crack propagation delay. This could be related with the consequence of the Dvorak theoretical model, which claims that: (i) the growth in the thinnest laminates is always stably along the thickness direction, and (2) unstably crack growths mostly occur as a tunneling crack along the width of the specimen.

Note however that two alternative theoretical models, incremental energy criterion [33] and finite frature mechanics [39, 28], explain the size effect assuming an abrupt onset of a crack with a finite length. The justification for this abrupt onset is the micromechanical transition from damage to crack. Some evidences can be observed here in the transition between a damage zone which span the whole thickness and after the first kink with a fast growth of the crack (particularly for $[0_2/90_2/0_2]$ and $[0_2/90_4/0_2]$). The

comprehensive study of this phenomenon, i.e. how abrupt is this crack growth, would require a robust dynamics analysis which falls beyond the scope of the present study.

Finally, within this context, it is worth mentioning the existence of a different theoretical model which relies on the Weibull statistical theory in order to provide a plausible argument to this *in-situ* strength effect, see [40]. This model bases the explanation of the size effect on the presence of flaws of a size statistically distributed per unit of volume. Basically, since thicker layers are characterized by larger volumes, they posses a higher probability for the presence of larger flaws. Note however that since the analysis presented here is purely deterministic and no dispersion on the material properties have been introduced, this model cannot be properly evaluated and discussed within the context of the present study.

5. Conclusions

In this work, a micro-mechanical analysis of fracture events in cross-ply laminates under in-plane monotonic loading has been conducted. The main focus of the current investigation concerned the investigation of scale effects in such specimens using computational micromechanics. For this purpose, multi-scale embedded models have been generating via the reproduction of the fibre internal arrangements of the specimens reported in [62].

Differing from alternative studies, the current numerical strategies encompassed the combined use of the CZM and the PF approach of fracture for respectively triggering failure events at fiber-matrix and within the matrix. The adaption of such numerical tools ensured the simultaneously accounting for critical elastic energy release rate and critical stress.

The emphasis of the analysis has been devoted to the careful identification of the different phases of failure events within the specimens in conjunction with the study of the analysis of the 90° layer thickness on the onset of progression of though-the-thickness crack, which has a strong connection to the so-called *in-situ* strength effect in fibrous composite materials.

Current predictions exhibited a closed qualitative agreement with respect to the experimental data available in the related literature, see [56, 36, 28]. The proposed numerical technique enable the consistent capturing of the sequence of damage events in laminates of the family $[0^\circ_2/90^\circ_n/0^\circ_2]$, with n=2, 4 and 8. In particular, it has been identified that the first damage mechanisms correspond to fibre-matrix decohesion events. Upon loading progression such phenomena coalesced leading to the generation of transverse through-the-thickness cracks within the matrix. Actual crack paths strongly depends on the particular fibre distributions, leading to possible branching and coalescence scenarios specially in thick laminates. This was in good agreement with respect to the experimental data. Nevertheless, present predictions presented deviations with respect to the strain levels at which these phenomena occurred. These differences are mainly attributed to possible 3D effects that have not been taken into consideration in the present 2D modeling framework.

With respect to the analysis of the *in-situ* strength effect in these specimens, it was found that the current numerical technique was in good agreement with the trend introduced by Dvorak's [22, 23, 24] in terms of through-the-thickness fracture propagation based on the thickness of the central 90° layer. analyzing the current numerical data, we observed a clear cracking propagation delay within the matrix for the thinnest specimen, which caused the increase in the apparent critical strain for the development through-the-thickness in comparison with the other two configurations.

Finally, it is worth mentioning that current results evidenced the strong potential of the proposed numerical framework comprising: (*i*) the use of physically-based fracture modeling capabilities that properly accounted for capturing size effects in engineering, which cannot be retrieved using Griffith-based theories, Linear Elastic Fracture Mechanics and stress-based damage capabilities, among others, (*ii*) its inherent versatility for triggering very complex fracture phenomena with reduced mesh-dependent pathology and without remarkable limitations in terms of geometry and constitutive laws at the material level. These attributes motivate the developments of further enhancement of the current framework to investigate additional cracking events in composite materials at different scales. Thus, in future investigations, the current model would include an interface between 0°- 90° plies for capturing scenarios with regard to the delamination or penetration into the 0° ply of the transverse matrix crack. In addition to the previous comments, an additional prospective activity of notable importance is the application

of the present methodology in 3D problems in order to capture tunneling effects. This requires the use of HPC architectures, being currently generated exploiting different phase field formulations [72, 71]. Moreover, from a modeling standpoint, several future extensions are worth to be explored. First, a dynamic model could be required to study the stability of the process of transition from damage to cracking, owing to the dynamic character of such phenomenon. Second, the inclusion of the matrix plastic behaviour would deserve a special attention, specifically for the incorporation of thermoplastic-based polymeric matrices and potentially the investigation of alternative composite materials, such as short fibre reinforced polymeric (SFRP) composites [16, 19, 18], among many others. These further developments are within the scope of including additional nonlinear effects in high-fidelity micromechanics ranging from the previously mentioned plastic-character of the matrix [17] to capturing fatigue-induced cracking events within the framework of the phase field method [37].

Acknowledgements

JR and IGG ackowledge the Consejería de Economía y Conocimiento of the Junta de Andalucía (Spain) for financial support under the contract US-1265577 that belongs to the Programa Operativo FEDER Andalucía 2014-2020. MP appreciates the financial support from the Italian Ministry of Education, University and Research (MIUR) to the research project of relevant national interest (PRIN 2017) XFAST-SIMS: Extra fast and accurate simulation of complex structural systems (Prot. 20173C478N).

References

[1] Aldakheel, F. [2020], 'A microscale model for concrete failure in poro-elasto-plastic media', *Theoretical and Applied Fracture Mechanics* **107**, 102517.
URL: *http://www.sciencedirect.com/science/article/pii/S0167844219307591*

[2] Amacher, R., Cugnoni, J., Botsis, J., Sorensen, L., Smith, W. and Dransfeld, C. [2014], 'Thin ply composites: experimental characterization and modeling of size-effects', *Composites Science and Technology* **101**, 121–132.

[3] Arteiro, A., Catalanotti, G., Melro, A., Linde, P. and Camanho, P. [2015*a*], 'Micro-mechanical analysis of the effect of ply thickness on the transverse compressive strength of polymer composites', *Composites Part A: Applied Science and Manufacturing* **79**, 127–137.

[4] Arteiro, A., Catalanotti, G., Melro, A., Linde, P. and Camanho, P. P. [2014], 'Micro-mechanical analysis of the in situ effect in polymer composite laminates', *Composite Structures* **116**, 827–840.

[5] Arteiro, A., Catalanotti, G., Melro, A. R., Linde, P. and Camanho, P. P. [2015*b*], 'Micro-mechanical analysis of the effect of ply thickness on the transverse compressive strength of polymer composites', *Composites Part A: Applied Science and Manufacturing* **79**, 127–137.

[6] Aveston, J. [1971], The properties of fiber composites, *in* 'Conf. Proc. National Physical Lab., 1971', IPC Science and Technology Press.

[7] Berthelot, J. [2003], 'Transverse cracking and delamination in cross-ply glass-fiber and carbon-fiber reinforced plastic laminates: Static and fatigue loading', *Applied Mechanics Reviews* **56**(1), 111–147.

[8] Bourdin, B., Francfort, G. A. and Marigo, J.-J. [2000*a*], 'Numerical experiments in revisited brittle fracture', *Journal of the Mechanics and Physics of Solids* **48**(4), 797–826.

[9] Bourdin, B., Francfort, G. A. and Marigo, J.-J. [2000*b*], 'Numerical experiments in revisited brittle fracture', *Journal of the Mechanics and Physics of Solids* **48**(4), 797–826.

[10] Camanho, P., Maim, P. and Dvila, C. [2007], 'Prediction of size effects in notched laminates using continuum damage mechanics', *Composites Science and Technology* **67**(13), 2715 – 2727.

[11] Camanho, P. P., Dávila, C. G., Pinho, S. T., Iannucci, L. and Robinson, P. [2006], 'Prediction of in situ strengths and matrix cracking in composites under transverse tension and in-plane shear', *Composites Part A: Applied Science and Manufacturing* **37**(2), 165–176.

[12] Carollo, V., Reinoso, J. and Paggi, M. [2017], 'A 3d finite strain model for intralayer and interlayer crack simulation coupling the phase field approach and cohesive zone model', *Composite Structures* **182**, 636 – 651.

[13] Carollo, V., Reinoso, J. and Paggi, M. [2018], 'Modeling complex crack paths in ceramic laminates: A novel variational framework combining the phase field method of fracture and the cohesive zone model', *Journal of the European Ceramic Society* **38**(8), 2994 – 3003. Cermodel 2017: Modelling and Simulation Meet Innovation in Ceramics Technology.

[14] Cornetti, P., Sapora, A. and Carpinteri, A. [2016], 'Short cracks and v-notches: Finite fracture mechanics vs. cohesive crack model', *Engineering Fracture Mechanics* **168**, 2 – 12.

[15] Correa, E., París, F. and Mantič, V. [2013], 'Effect of the presence of a secondary transverse load on the inter-fibre failure under tension', *Engineering Fracture Mechanics* **103**, 174 – 189.

[16] Dean, A., Grbic, N., Rolfes, R. and Behrens, B. [2019], 'Macro-mechanical modeling and experimental validation of anisotropic, pressure- and temperature-dependent behavior of short fiber composites', *Composite Structures* **211**, 630 – 643.
URL: *http://www.sciencedirect.com/science/article/pii/S0263822318338613*

[17] Dean, A., Reinoso, J., Jha, N., Mahdi, E. and Rolfes, R. [2020], 'A phase field approach for ductile fracture of short fibre reinforced composites', *Theoretical and Applied Fracture Mechanics* **106**, 102495.
URL: *http://www.sciencedirect.com/science/article/pii/S0167844219306536*

[18] Dean, A., Reinoso, J., Sahraee, S. and Rolfes, R. [2016], 'An invariant-based anisotropic material model for short fiber-reinforced thermoplastics: Coupled thermo-plastic formulation', *Composites Part A: Applied Science and Manufacturing* **90**, 186–199.

[19] Dean, A., Sahraee, S., Reinoso, J. and Rolfes, R. [2016], 'Finite deformation model for short fibre reinforced composites: Application to hybrid metal-composite clinching joints', *Composite Structures* **150**, 162–171.

[20] Di Stasio, L., Varna, J. and Ayadi, Z. [2019], 'Energy release rate of the fiber/matrix interface crack in ud composites under transverse loading: effect of the fiber volume fraction and of the distance to the free surface and to non-adjacent debonds', *Theoretical and Applied Fracture Mechanics* p. 102251.

[21] Dittmann, M., Aldakheel, F., Schulte, J., Wriggers, P. and Hesch, C. [2018], 'Variational phase-field formulation of non-linear ductile fracture', *Computer Methods in Applied Mechanics and Engineering* **342**, 71 – 94.
URL: *http://www.sciencedirect.com/science/article/pii/S0045782518303621*

[22] Dvorak, G. [2012], *Micromechanics of composite materials*, Vol. 186, Springer Science & Business Media.

[23] Dvorak, G. J. and Laws, N. [1985], 'Mechanics of first ply failure in composite laminates', *American Society of Mechanical Engineers, Applied Mechanics Division* **74**, 59–69.

[24] Dvorak, G. J. and Laws, N. [1986], 'Analysis of first ply failure in composite laminates', *Engineering Fracture Mechanics* **25**(5-6), 763–770.

[25] García, I. G., Mantič, V. and Graciani, E. [2015], 'Debonding at the fibre-matrix interface under remote transverse tension. One debond or two symmetric debonds?', *European Journal of Mechanics, A/Solids* **53**, 75–88.

[26] García, I. G., Mantič, V. and Blázquez, A. [2018], 'The effect of residual thermal stresses on transverse cracking in cross-ply laminates. An application of the Coupled Criterion of the Finite Fracture Mechanics', *International Journal of Fracture* **211**, 61–74.

[27] García, I., Justo, J., Simon, A. and Mantič, V. [2019], 'Experimental study of the size effect on transverse cracking in cross-ply laminates and comparison with the main theoretical models', *Mechanics of Materials* **128**, 24 – 37.

[28] García, I., Mantič, V., Blázquez, A. and París, F. [2014], 'Transverse crack onset and growth in cross-ply [0/90] s laminates under tension. application of a coupled stress and energy criterion', *International journal of Solids and Structures* **51**(23-24), 3844–3856.

[29] Garrett, K. and Bailey, J. [1977], 'Multiple transverse fracture in 90 cross-ply laminates of a glass fibre-reinforced polyester', *Journal of materials science* **12**(1), 157–168.

[30] Gerasimov, T. and Lorenzis, L. D. [2019], 'On penalization in variational phase-field models of brittle fracture', *Computer Methods in Applied Mechanics and Engineering* **354**, 990 – 1026.

[31] Goodier, J. [1933], 'Concentration of stress around spherical and cylindrical inclusions and flaws', *Journal of Applied Mechanics* **55**, 39–44.

[32] Guillén-Hernández, T., García, I. G., Reinoso, J. and Paggi, M. [2019], 'A micromechanical analysis of inter-fiber failure in long reinforced composites based on the phase field approach of fracture combined with the cohesive zone model', *International Journal of Fracture* .
URL: *https://doi.org/10.1007/s10704-019-00384-8*

[33] Hashin, Z. [1996], 'Finite thermoelastic fracture criterion with application to laminate cracking analysis', *Journal of the Mechanics and Physics of Solids* **44**(7), 1129–1145.

[34] Herráez, M., Mora, D., Naya, F., Lopes, C. S., González, C. and LLorca, J. [2015], 'Transverse cracking of cross-ply laminates: A computational micromechanics perspective', *Composites Science and Technology* **110**, 196–204.

[35] Kiendl, J., Ambati, M., De Lorenzis, L., Gomez, H. and Reali, A. [2016], 'Phase-field description of brittle fracture in plates and shells', *Computer Methods in Applied Mechanics and Engineering* **312**, 374–394.

[36] Kohler, S., Cugnoni, J., Amacher, R. and Botsis, J. [2019], 'Transverse cracking in the bulk and at the free edge of thin-ply composites: experiments and multiscale modelling', *Composites Part A: Applied Science and Manufacturing* .

[37] Kristensen, P. K. and Martnez-Paeda, E. [2020], 'Phase field fracture modelling using quasi-newton methods and a new adaptive step scheme', *Theoretical and Applied Fracture Mechanics* **107**, 102446.
URL: *http://www.sciencedirect.com/science/article/pii/S0167844219305580*

[38] Kumar, A. and Lopez-Pamies, O. [2020], 'The phase-field approach to self-healable fracture of elastomers: A model accounting for fracture nucleation at large, with application to a class of conspicuous experiments', *Theoretical and Applied Fracture Mechanics* **107**, 102550.
URL: *http://www.sciencedirect.com/science/article/pii/S0167844219307566*

[39] Leguillon, D. [2002], 'Strength or toughness? A criterion for crack onset at a notch', *European Journal of Mechanics and Solids* **21**(1), 61–72.

[40] Li, D. S. and Wisnom, M. R. [1997], 'Evaluating weibull parameters for transverse cracking in cross-ply laminates', *Journal of composite materials* **31**(9), 935–951.

[41] Maimı, P., Camanho, P., Mayugo, J. and Turon, A. [2011], 'Matrix cracking and delamination in laminated composites. part i: Ply constitutive law, first ply failure and onset of delamination', *Mechanics of materials* **43**(4), 169–185.

[42] Mantič, V. [2009], 'Interface crack onset at a circular cylindrical inclusion under a remote transverse tension. application of a coupled stress and energy criterion', *International journal of Solids and Structures* **46**(6), 1287–1304.

[43] Mantič, V. and García, I. G. [2012], 'Crack onset and growth at the fibre-matrix interface under a remote biaxial transverse load. Application of a coupled stress and energy criterion', *International Journal of Solids and Structures* **49**(17), 2273–2290.

[44] Martnez-Paeda, E., Golahmar, A. and Niordson, C. F. [2018], 'A phase field formulation for hydrogen assisted cracking', *Computer Methods in Applied Mechanics and Engineering* **342**, 742 – 761.

URL: *http://www.sciencedirect.com/science/article/pii/S0045782518303529*

[45] Melro, A. R., Camanho, P. P., Andrade Pires, F. M. and Pinho, S. T. [2013], 'Micromechanical analysis of polymer composites reinforced by unidirectional fibres: Part II-Micromechanical analyses', *International Journal of Solids and Structures* **50**(11-12), 1906–1915.

[46] Miehe, C., Hofacker, M. and Welschinger, F. [2010], 'A phase field model for rate-independent crack propagation: Robust algorithmic implementation based on operator splits', *Computer Methods in Applied Mechanics and Engineering* **199**(45-48), 2765–2778.

[47] Miehe, C., Kienle, D., Aldakheel, F. and Teichtmeister, S. [2016], 'Phase field modeling of fracture in porous plasticity: A variational gradient-extended eulerian framework for the macroscopic analysis of ductile failure', *Computer Methods in Applied Mechanics and Engineering* **312**, 3 – 50. Phase Field Approaches to Fracture.
URL: *http://www.sciencedirect.com/science/article/pii/S0045782516305412*

[48] Miehe, C., Welschinger, F. and Hofacker, M. [2010], 'Thermodynamically consistent phase-field models of fracture: Variational principles and multi-field fe implementations', *International Journal for Numerical Methods in Engineering* **83**(10), 1273–1311.

[49] Natarajan, S., Annabattula, R. K., Martínez-Pañeda, E. et al. [2019], 'Phase field modelling of crack propagation in functionally graded materials', *Composites Part B: Engineering* **169**, 239–248.

[50] Nguyen, T.-T., Yvonnet, J., Zhu, Q.-Z., Bornert, M. and Chateau, C. [2016], 'A phase-field method for computational modeling of interfacial damage interacting with crack propagation in realistic microstructures obtained by microtomography', *Computer Methods in Applied Mechanics and Engineering* **312**, 567–595.

[51] Noii, N., Aldakheel, F., Wick, T. and Wriggers, P. [2020], 'An adaptive globallocal approach for phase-field modeling of anisotropic brittle fracture', *Computer Methods in Applied Mechanics and Engineering* **361**, 112744.
URL: *http://www.sciencedirect.com/science/article/pii/S0045782519306346*

[52] Okabe, T., Imamura, H., Sato, Y., Higuchi, R., Koyanagi, J. and Talreja, R. [2015], 'Experimental and numerical studies of initial cracking in CFRP cross-ply laminates', **68**, 81–89.

[53] Okabe, T., Sekine, H., Noda, J., Nishikawa, M. and Takeda, N. [2004], 'Characterization of tensile damage and strength in GFRP cross-ply laminates', *Materials Science and Engineering: A* **383**(2), 381–389.

[54] Paggi, M. and Reinoso, J. [2017], 'Revisiting the problem of a crack impinging on an interface:a modeling framework for the interaction between the phase field approach for brittle fracture and the interface cohesive zone model', *Computer Methods in Applied Mechanics and Engineering* **321**, 145 – 172.

[55] París, F., Velasco, M. L. and Correa, E. [2018], 'Micromechanical study on the influence of scale effect in the first stage of damage in composites', *Composites Science and Technology* **160**, 1–8.

[56] Parvizi, A., Garrett, K. and Bailey, J. [1978], 'Constrained cracking in glass fibre-reinforced epoxy cross-ply laminates', *Journal of Materials Science* **13**(1), 195–201.

[57] Quintanas-Corominas, A., Maimí, P., Casoni, E., Turon, A., Mayugo, J., Guillamet, G. and Vázquez, M. [2018], 'A 3D transversally isotropic constitutive model for advanced composites implemented in a high performance computing code', *European Journal of Mechanics - A/Solids* **71**, 278 – 291.

[58] Quintanas-Corominas, A., Reinoso, J., Casoni, E., Turon, A. and Mayugo, J. [2019], 'A phase field approach to simulate intralaminar and translaminar fracture in long fiber composite materials', *Composite Structures* .

[59] Reinoso, J., Catalanotti, G., Blázquez, A., Areias, P., Camanho, P. and París, F. [2017], 'A consistent anisotropic damage model for laminated fiber-reinforced composites using the 3d-version of the puck failure criterion', *International Journal of Solids and Structures* pp. 37 – 53.

[60] Reinoso, J. and Paggi, M. [2014], 'A consistent interface element formulation for geometrical and material nonlinearities', *Computational Mechanics* **54**(6), 1569–1581.

[61] Russ, J., Slesarenko, V., Rudykh, S. and Waisman, H. [2020], 'Rupture of 3d-printed hyperelastic composites: experiments and phase field fracture modeling', *Journal of the Mechanics and Physics of Solids* p. 103941.
URL: *http://www.sciencedirect.com/science/article/pii/S0022509620301770*

[62] Saito, H., Takeuchi, H. and Kimpara, I. [2012], 'Experimental evaluation of the damage growth restraining in 90 layer of thin-ply cfrp cross-ply laminates', *Advanced Composite Materials* **21**(1), 57–66.

[63] Sandino, C., Correa, E. and Pars, F. [2018], 'A study of the influence of a nearby fibre on the interface crack growth under transverse compression in composite materials', *Engineering Fracture Mechanics* **193**, 1 – 16.

[64] Sebaey, T., Costa, J., Maimí, P., Batista, Y., Blanco, N. and Mayugo, J. [2014], 'Measurement of the in situ transverse tensile strength of composite plies by means of the real time monitoring of microcracking', *Composites Part B: Engineering* **65**, 40–46.

[65] Sorensen, B. and Talreja, R. [1993], 'Effects of nonuniformity of fiber distribution on thermally-induced residual stresses and cracking in ceramic matrix composites', *Mechanics of Materials* **16**(4), 351 – 363.

[66] Tanné, E., Li, T., Bourdin, B., Marigo, J.-J. and Maurini, C. [2018], 'Crack nucleation in variational phase-field models of brittle fracture', *Journal of the Mechanics and Physics of Solids* **110**, 80 – 99.

[67] Toya, M. [1973], 'A crack along the interface of a rigid circular inclusion embedded in an elastic solid', *International Journal of Fracture* **9**(4), 463–470.

[68] Turon, A., Camanho, P., Costa, J. and Dávila, C. [2006], 'A damage model for the simulation of delamination in advanced composites under variable-mode loading', *Mechanics of Materials* **38**(11), 1072 – 1089.

[69] Turon, A., Dávila, C., Camanho, P. and Costa, J. [2007], 'An engineering solution for mesh size effects in the simulation of delamination using cohesive zone models', *Engineering Fracture Mechanics* **74**(10), 1665 – 1682.

[70] Wisnom, M. [2000], 'Size effects in composites'.

[71] Wu, J. [2017], 'A unified phase-field theory for the mechanics of damage and quasi-brittle failure', *Journal of the Mechanics and Physics of Solids* **103**, 72–99.

[72] Wu, J. and Nguyen, V. [2018], 'A length scale insensitive phase-field damage model for brittle fracture', *Journal of the Mechanics and Physics of Solids* **119**, 20–42.

[73] Zhang, X., Krischok, A. and Linder, C. [2016], 'A variational framework to model diffusion induced large plastic deformation and phase field fracture during initial two-phase lithiation of silicon electrodes', *Computer Methods in Applied Mechanics and Engineering* **312**, 51 – 77.

[74] Zhuang, L., Pupurs, A., Varna, J., Talreja, R. and Ayadi, Z. [2018], 'Effects of inter-fiber spacing on fiber-matrix debond crack growth in unidirectional composites under transverse loading', *Composites Part A: Applied Science and Manufacturing* **109**, 463–471.